Mechanochemically assisted synthesis and visible light photocatalytic properties of lanthanum nickel oxide nanoparticles

Mechanochemically assisted synthesis and visible light photocatalytic properties of lanthanum nickel oxide nanoparticles

Tomohiro Iwasaki *, Yasuyuki Shimamura, Yuri Makino, Satoru Watano

Department of Chemical Engineering, Osaka Prefecture University, Sakai, Osaka 599-8531, Japan

* Corresponding author. Tel: +81 72 254 9307; fax: +81 72 254 9911.

E-mail address: iwasaki@chemeng.osakafu-u.ac.jp (T. Iwasaki).

Abstract

Perovskite-type lanthanum nickel oxide (lanthanum nickelate, $LaNiO_3$) nanoparticles with high photocatalytic activity were synthesized via a mechanochemical route. A high-energy planetary ball mill was employed for mechanochemical preparation of an activated precursor of $LaNiO_3$ via a solid-state reaction of $LaCl_3$, $NiCl_2$, and NaOH. The mechanochemical treatment was performed for 1 h at a revolution speed of the milling pot of 600 rpm. In comparison to an un-milled precursor, a simple mixture of $La(OH)_3$, $Ni(OH)_2$, and NaCl, the activated precursor demonstrated that the mechanochemical treatment contributes to the formation of $LaNiO_3$ at low temperatures. This effect, in turn, leads to reduction of the optical band gap, i.e., enhancement of the visible light photocatalytic activity. Standard characterization techniques confirmed that crystalline round $LaNiO_3$ nanoparticles with a median diameter of 46 nm, a surface area of 23 m^2/g, and an optical band gap of 1.09 eV were obtained after calcination of the mechanochemically treated precursor at 873 K for 1 h. The visible-light-driven

photocatalytic activity was evaluated based on the photodegradation of methyl orange in an aqueous solution. The $LaNiO_3$ catalyst nanoparticles efficiently decomposed methyl orange under visible light irradiation; more than 99% of methyl orange was removed from the solution in 2 h, indicating that the $LaNiO_3$ nanoparticles possess good photocatalytic properties.

Keywords: $LaNiO_3$ nanoparticles; Perovskite; Mechanochemical reaction; High-energy ball milling; Visible-light-driven photocatalytic activity

1. Introduction

Lanthanum nickel oxide (lanthanum nickelate, $LaNiO_3$) with a perovskite-type structure has attracted considerable attention in multiple fields. For example, $LaNiO_3$ is a promising candidate as an electrode constituent material due to excellent electrical properties [1–3]. Additionally, $LaNiO_3$ and its derived materials have been used as catalysts because they show high catalytic activity in several chemical reactions, such as the evolution of hydrogen gas from organic compounds [4–8]. Particularly, the visible-light-driven photocatalytic activity of $LaNiO_3$ has lately received particular attention in the degradation of organic compounds [9–11] and hydrogen production [12,13].

$LaNiO_3$ has been synthesized using various techniques, such as sol-gel [5,10,12,13], combustion [1,6,8,9,14–17], hydrothermal [7,18], microwave heating [19], spray pyrolysis [4], reverse microemulsion [11], polymerization [20], and molten salt [21]. These methods often require relatively long reaction times and/or high reaction temperatures. In contrast, mechanochemically assisted synthesis methods that use

high-energy milling to prepare a precursor effectively reduce the reaction time and temperature in the synthesis of perovskite-type oxides [22–27]. To the best of our knowledge, mechanochemical synthesis of $LaNiO_3$ has not been published to date.

This study investigated the mechanochemical effects of the precursor preparation on the formation and properties of $LaNiO_3$ nanoparticles. The visible-light-driven photocatalytic activity of the obtained $LaNiO_3$ nanoparticles was subsequently examined.

2. Experimental

2.1. Preparation of precursor and $LaNiO_3$

Chemicals of analytical grade were purchased from Wako Pure Chemical Industries and used as received without further purification. A high-energy planetary ball mill (Pulverisette 6, Fritsch) was employed to prepare a precursor of $LaNiO_3$. A powder mixture consisting of 5 mmol of $LaCl_3 \cdot 7H_2O$, 5 mmol of $NiCl_2 \cdot 6H_2O$, and 25 mmol of NaOH was placed in a zirconia pot of 45 cm^3 inner volume together with 18 zirconia balls of 10 mm diameter. The ball-to-powder mass ratio was 14:1, and the atmosphere in the pot was air. The revolution speed of the pot was 600 rpm, and the milling time was 1 h. The mechanochemical treatment of the starting materials produced a gray paste as the precursor, according to the following solid-state reaction.

$$LaCl_3 \cdot 7H_2O + NiCl_2 \cdot 6H_2O + 5NaOH \rightarrow La(OH)_3 + Ni(OH)_2 + 5NaCl + 13H_2O \quad (1)$$

The resulting paste was removed from the pot and dried overnight at 383 K in air. The obtained precursor powder was hereafter denoted as the MC precursor. The MC precursor was calcined in an electric furnace for 1 h in air, which formed $LaNiO_3$

according to the following solid phase reaction.

$$La(OH)_3 + Ni(OH)_2 + (1/4)O_2 \rightarrow LaNiO_3 + (5/2)H_2O \quad (2)$$

The calcination temperature was varied between 773 K and 973 K, and the heating rate was fixed at 10 K/min. The resultant black powder was washed three times with deionized water to remove NaCl and dried at 383 K to obtain the final product.

In order to confirm the mechanochemical effects on precursor formation, a simple powder mixture of $La(OH)_3$, $Ni(OH)_2$ and NaCl as the precursor was prepared by coprecipitation as follows: 6 mmol of $LaCl_3 \cdot 7H_2O$, 6 mmol of $NiCl_2 \cdot 6H_2O$, and 30 mmol of NaOH were dissolved in 70 mL of deionized water, and the precipitate of $La(OH)_3$ and $Ni(OH)_2$ was formed in the solution. The water was evaporated at 383 K, and a light green powder consisting of $La(OH)_3$, $Ni(OH)_2$ and NaCl was obtained. The un-milled precursor powder thus prepared was denoted as the UM precursor. The UM precursor was also calcined at temperatures between 873 K and 1073 K for 1 h in air. After removing NaCl by washing with deionized water, the final product was obtained.

2.2. Characterization

The Fourier transform infrared (FT-IR) spectra of the MC and UM precursors were recorded on a spectrophotometer (IRAffinity-1, Shimadzu). The thermogravimetric and differential thermal analysis (TG-DTA) curves of the precursors were measured from ambient to 1050 K (heating rate: 10 K/min) in an air flow rate of 100 mL/min with a thermal analyzer (DTG-60, Shimadzu) to investigate the reaction behavior of precursors during calcination. The powder X-ray diffraction (XRD) patterns of precursors and final products were obtained on an X-ray diffractometer (RINT-1500, Rigaku) using CuKα

radiation at 40 kV and 80 mA. The average crystallite sizes of $LaNiO_3$ in the final products were determined using Scherrer's equation. The *a*- and *c*-axes lattice parameters (*a* and *c*, respectively) were also calculated, assuming that the obtained $LaNiO_3$ had a hexagonal structure. The diffuse reflectance UV-visible spectra of final products were measured by a spectrophotometer with an integrating sphere (UV-2600, Shimadzu) to determine the optical band gap by drawing the Tauc plot.

The morphology of the $LaNiO_3$ nanoparticles derived from the mechanochemically treated precursor calcined at 873 K was imaged by field emission scanning electron microscopy (FE-SEM; JSM-6700F, JEOL) operated at an accelerating voltage of 15 kV. The chemical composition was determined by energy-dispersive X-ray spectroscopy (EDS; JED-2300F, JEOL) attached to the FE-SEM. The particle size distribution (number basis) was measured with a dynamic light scattering particle size analyzer (Zetasizer Nano ZS, Malvern). The specific surface area was determined by the Brunauer–Emmett–Teller (BET) method based on nitrogen gas adsorption using an automatic surface area analyzer (Betasorb Model 4200, Beta Scientific).

The visible-light-driven photocatalytic activity of the $LaNiO_3$ nanoparticles was evaluated through the decomposition of methyl orange (denoted as MO hereafter) in water [9,10]. Twenty milligrams of the catalyst powder was added to 10 mL of 10 mg/L MO solution. The resulting suspension was subjected to visible-light irradiation at room temperature with magnetic stirring. A 250 W halogen lamp was used as the light source. The distance from the halogen bulb to the suspension was fixed to 150 mm, and a cutoff filter that removed UV rays of wavelengths shorter than 410 nm was placed between the lamp and the suspension. At specific time intervals, the absorbance of the filtered supernatant was measured at 464 nm using a spectrophotometer (Ubest V-530, JASCO)

to determine the removal of MO defined by

$$\text{Removal [\%]} = [1-(C/C_0)]\times 100 \quad (3)$$

where C_0 and C are the concentrations of MO in the solution before and after visible-light irradiation, respectively. The removal of MO in the dark, i.e., the adsorption of MO onto the $LaNiO_3$ nanoparticles, was also measured as a control.

3. Results and discussion

3.1. Mechanochemical effects on formation of $LaNiO_3$

Figs. 1 and 2 show the FT-IR spectra and TG-DTA curves of the MC and UM precursors, respectively. The precursors had typical IR absorption bands at approximately 3450 and 1640 cm^{-1}, attributed to the O–H stretching and bending vibrations, respectively. The broad peak at approximately 630 cm^{-1} was assigned to the M–O (M = La and Ni) bond vibration [28,29]. The weak bands at approximately 1500 and 1390 cm^{-1} were attributed to carboxylate and carbonate species, respectively, originating from CO_2 in air [30]. In the FT-IR spectra there was no noticeable difference between the precursors. In contrast, as seen in Fig. 2, the TG-DTA curves of the precursors differed from each other. In particular, the thermal reaction behaviors between 500 K and 650 K and between 850 K and 950 K were noticeably different, likely due to the thermal dehydration of $La(OH)_3$ and $Ni(OH)_2$ and the formation of $LaNiO_3$, respectively. The latter result suggests that the MC precursor can provide $LaNiO_3$ at relatively low temperatures compared with the UM.

Fig. 3 shows the XRD patterns of precursors and final products calcined at different temperatures. The MC and UM precursors mainly consisted of $La(OH)_3$ (JCPDS

36-1481), $Ni(OH)_2$ (JCPDS 74-2075), and NaCl (JCPDS 05-0628), indicating that the mechanochemical reaction of $LaCl_3$, $NiCl_2$, and NaOH in Eq. (1) occurred in the preparation of MC precursor. However, the MC precursor contained relatively low-crystalline reactive components compared with the UM. The products after calcination of the precursors at a low temperature were determined to have minor phases of lanthanum carbonate compounds such as $LaCO_3OH$ (JCPDS 49-0981) and $La_2O_2CO_3$ (JCPDS 84-1963). Based on the FT-IR analysis results, the precursors could contain amorphous lanthanum carbonate compounds, although their distinct peaks were not observed in the XRD data. The XRD analysis also confirmed that $LaNiO_3$ (JCPDS 33-0711) can be formed by calcination of the MC and UM precursors at temperatures higher than 873 K and 973 K, respectively. This was in agreement with the TG-DTA results. Particularly, in the MC precursor, the reactants of relatively low crystallinity such as $La(OH)_3$ and $Ni(OH)_2$ could be microscopically homogeneously mixed during high-energy milling. This might lead to the activation of reactants, resulting in the formation of $LaNiO_3$ at relatively low temperatures. However, the products contained a small amount of NiO (JCPDS 47-1049), suggesting that amorphous lanthanum compounds (e.g., $La(OH)_3$, La_2O_3) were also present. Furthermore, a reaction between lanthanum carbonate compounds and nickel species may occur during calcination to form $LaNiO_3$. A better understanding of the activation and reaction mechanisms requires more precise investigation, which will be addressed in our future publications.

3.2. Characterization of $LaNiO_3$

Table 1 lists the properties of final products. We found that calcination at lower temperatures led to a reduction of the average crystallite size and band gap and to an

increase of the lattice parameters, implying that the optical band gap of $LaNiO_3$ depended strongly on the crystallinity and crystal structure. This was often observed in some alloys and semiconductors [31,32]. Accordingly, the mechanochemical treatment in the preparation of precursor can contribute to the formation of $LaNiO_3$ at low temperatures, which may result in reduction of the band gap, i.e., enhancement of the visible light photocatalytic activity. However, when the calcination temperature was 973 K, the MC precursor yielded a product with a smaller band gap compared with the UM, although there were no noticeable differences in the crystallite size and lattice parameters. This finding suggests that there is a mechanochemical effect on the band gap in addition to the reduction of $LaNiO_3$ formation temperature previously mentioned. Further studies on the mechanism are in progress and will be reported elsewhere.

Further analysis was performed on the product with the lowest band gap. Fig. 4 depicts a typical SEM image of this sample, confirming that it consisted of round nanoparticles with a diameter of approximately 30–70 nm. Fig. 5 shows the particle size distribution. The median diameter was found to be 46 nm. The BET specific surface area analysis indicated that this sample had a relatively large surface area of 23 m^2/g. Assuming that all of the particles were spherical and the density was 7.2 g/cm^3 [13,19], the average particle diameter was calculated to be 36 nm from the specific surface area, which was close to the median diameter but larger than the average crystallite size (9.4 nm). This finding implies that the $LaNiO_3$ nanoparticles were polycrystalline. As shown in Fig. 6, the EDS analysis confirmed that this sample contained 57.5 mass% La, 21.9 mass% Ni, 20.4 mass% O, and 0.2 mass% Zr, which suggested that the chemical formula was $LaNi_{0.9}O_{3.1}$ and that the contamination due to the wear of the pot and balls was small.

Fig. 7 shows the evaluation of the visible-light-induced photocatalytic properties of the $LaNiO_3$ sample. In the dark, approximately 20% of MO was removed from the solution by adsorption immediately after the sample was immersed in the solution, and the amount of removed MO then slightly increased as time elapsed. When the suspension was placed under visible light, in the initial stages (less than 15 min) the concentration of MO was almost the same as that in the dark because the photocatalytic decomposition of MO was relatively small compared to the adsorption. However, the rate of photocatalytic decomposition exceeded that of adsorption after 30 min, and MO was rapidly decomposed. Ultimately, 99.5% of MO was removed in 2 h, indicating good photocatalytic activity compared to photocatalysts prepared by conventional methods [9,10].

4. Conclusions

A crystalline perovskite-type $LaNiO_3$ nanopowder with a relatively large specific surface area was readily synthesized via the high-energy ball milling of the starting materials followed by the calcination of the resulting activated precursor. The resultant $LaNiO_3$ catalyst exhibited good visible-light-driven photocatalytic activity. The mechanochemical treatment of the precursor reduces the temperature required for $LaNiO_3$ formation, which leads to enhancement of the visible light photocatalytic activity. Furthermore, this mechanochemically assisted method can provide $LaNiO_3$ with high photocatalytic activity in a short period of time (i.e., 1 h of milling and 1 h of calcination) compared to conventional methods. The photocatalytic performance may be further enhanced by the optimization of the milling and calcination conditions.

References

[1] C.O. Soares, M.D. Carvalho, M.E. Melo Jorge, A. Gomes, R.A. Silva, C.M. Rangel M.I. da Silva Pereira, J. Appl. Electrochem. 42 (2012) 325–332.

[2] N. Sakamoto, K. Ozawa, T. Ohno, T. Kiguchi, T. Matsuda, T. Konno, N. Wakiya, H. Suzuki, J. Ceram. Soc. Jpn. 121 (2013) 619–622.

[3] Q. Xu, X. Han, F. Ding, L. Zhang, L. Sang, X. Liu, Q. Xu, J. Alloys Compd. 664 (2016) 750–755.

[4] R. Pereñíguez, V.M. González-DelaCruz, J.P. Holgado, A. Caballero, Appl. Catal. B 93 (2010) 346–353.

[5] A. Jahangiri, H. Pahlavanzadeh, H. Aghabozorg, Int. J. Hydrog. Energy 37 (2012) 9977–9984.

[6] J.C. Santos, M.J.B. Souza, J.A.C. Ruiz, D.M.A. Melo, M.E. Mesquita, A.M. Garrido Pedrosa, J. Braz. Chem. Soc. 23 (2012) 1858–1862.

[7] K.H. Lin, C.B. Wang, S.H. Chien, Int. J. Hydrog. Energy 38 (2013) 3226–3232.

[8] C.A. Franchini, W. Aranzaez, A.M. Duarte de Farias, G. Pecchi, M.A. Fraga, Appl. Catal. B 147 (2014) 193–202.

[9] Y. Li, S. Yao, W. Wen, L. Xue, Y. Yan, J. Alloys Compd. 491 (2010) 560–564.

[10] P. Tang, H. Sun, F. Cao, J. Yang, S. Ni, H. Chen, Adv. Mater. Res. 279 (2011) 83–87.

[11] D. Aman, T. Zaki, S. Mikhail, S.A. Selim, Catal. Today 164 (2011) 209–213.

[12] L. Jia, J. Li, W. Fang, J. Alloys Compd. 489 (2010) L13–L16.

[13] M. Khettab, S. Omeiri, D. Sellam, M.A. Ladjouzi, M. Trari, Mater. Chem. Phys. 132 (2012) 625–630.

[14] N.T.H. Le, J.M. Calderón-Moreno, M. Popa, D. Crespo, L. Van Hong, N.X. Phuc, J.

Eur. Ceram. Soc. 26 (2006) 403–407.

[15] Y. Wang, J. Zhu, X. Yang, L. Lu, X. Wang, Mater. Res. Bull. 41 (2006) 1565–1570.

[16] M. Kuras, R. Roucou, C. Petit, J. Mol. Catal. A 265 (2007) 209–217.

[17] M. Biswas, J. Alloys Compd. 480 (2009) 942–946.

[18] D.V. Dharmadhikari, A.A. Athawale, AIP Conf. Proc. 1536 (2013) 1017–1018.

[19] A. Galal, N.F. Atta, S.M. Ali, Appl. Catal. A 409–410 (2011) 202–208.

[20] J.D.G. Fernandes, D.M.A. Melo, L.B. Zinner, C.M. Salustiano, Z.R. Silva, A.E. Martinelli, M. Cerqueira, C. Alves Júnior, E. Longo, M.I.B. Bernardi, Mater. Lett. 53 (2002) 122–125.

[21] J. Yang, R. Li, J. Zhou, X. Li, Y. Zhang, Y. Long, Y. Li, J. Alloys Compd. 508 (2010) 301–308.

[22] Q. Zhang, F Saito, Adv. Powder Technol. 23 (2012) 523–531.

[23] L Zhang, Z Xu, L Cao, X Yao, Mater. Lett. 61 (2007) 1130–1133.

[24] Q Li, Z Wang, Y Yang, Mater. Lett. 63 (2009) 2297–2299.

[25] F. Saito, Q. Zhang, J. Kano, J. Mater. Sci. 39 (2004) 5051–5055.

[26] S. Sompech, A. Srion, A. Nuntiya, ScienceAsia 38 (2012) 102–107

[27] K. Samuvel, K. Ramachandran, Optik 127 (2016) 1781–1786.

[28] M. Aghazadeh, A.N. Golikand, M. Ghaemi, T. Yousefi, J. Electrochem. Soc. 158 (2011) E136–E141.

[29] G. Fu, Z. Hu, L. Xie, X. Jin, Y. Xie, Y. Wang, Z. Zhang, Y. Yang, H. Wu, Int. J. Electrochem. Sci. 4 (2009) 1052–1062.

[30] Z. Xu, S. Bian, J. Wang, T. Liu, L. Wang, Y. Gao, RSC Adv. 3 (2013) 1410–1419.

[31] I. Vurgaftman, J.R. Meyer, L.R. Ram-Mohan, J. Appl. Phys. 89 (2001) 5815–5875.

[32] C. Besleaga, A.C. Galca, C.F. Miclea, I. Mercioniu, M. Enculescu, G.E. Stan, A.O.

Mateescu, V. Dumitru, S. Costea, J. Appl. Phys. 116 (2014) 153509.

Table and Figure captions

Table 1 Properties of final products derived from MC and UM precursors

Fig. 1. FT-IR spectra of (a) MC and (b) UM precursors.

Fig. 2. TG-DTA curves of (a) MC and (b) UM precursors.

Fig. 3. XRD patterns of final products after calcination of (a) MC and (b) UM precursors at different temperatures.

Fig. 4. Typical SEM image of final product derived from MC precursor after calcination at 873 K.

Fig. 5. Particle size distribution of final product derived from MC precursor after calcination at 873 K.

Fig. 6. EDS spectrum of final product derived from MC precursor after calcination at 873 K.

Fig. 7. Removal of MO (a) in the dark and (b) under visible light irradiation using final product derived from MC precursor after calcination at 873 K.

Table 1 Properties of final products derived from MC and UM precursors

Precursors	Calcination temperature [K]	Average crystallite size [nm]	Lattice parameters		Band gap [eV]
			a [Å]	*c* [Å]	
MC	873	9.4	5.498	6.623	1.09
MC	973	12.1	5.484	6.603	1.14
UM	973	12.7	5.475	6.598	2.78
UM	1073	22.3	5.463	6.570	3.16

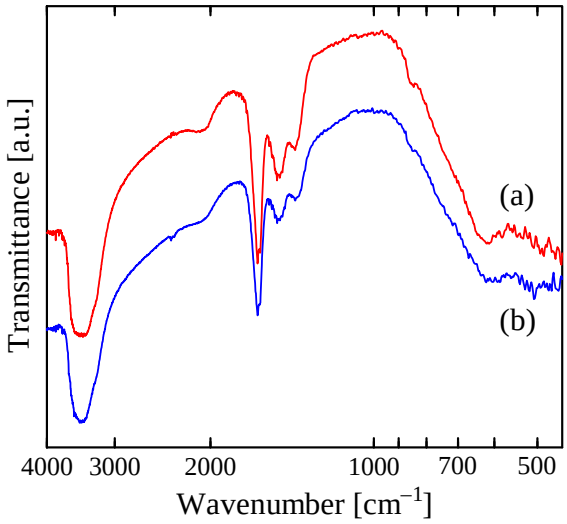

Fig. 1. FT-IR spectra of (a) MC and (b) UM precursors.

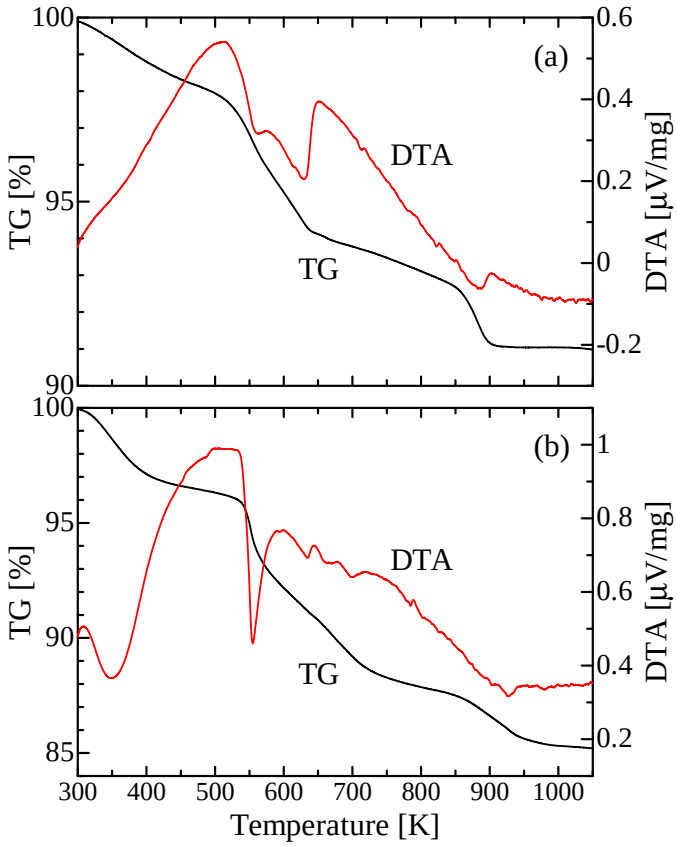

Fig. 2. TG-DTA curves of (a) MC and (b) UM precursors.

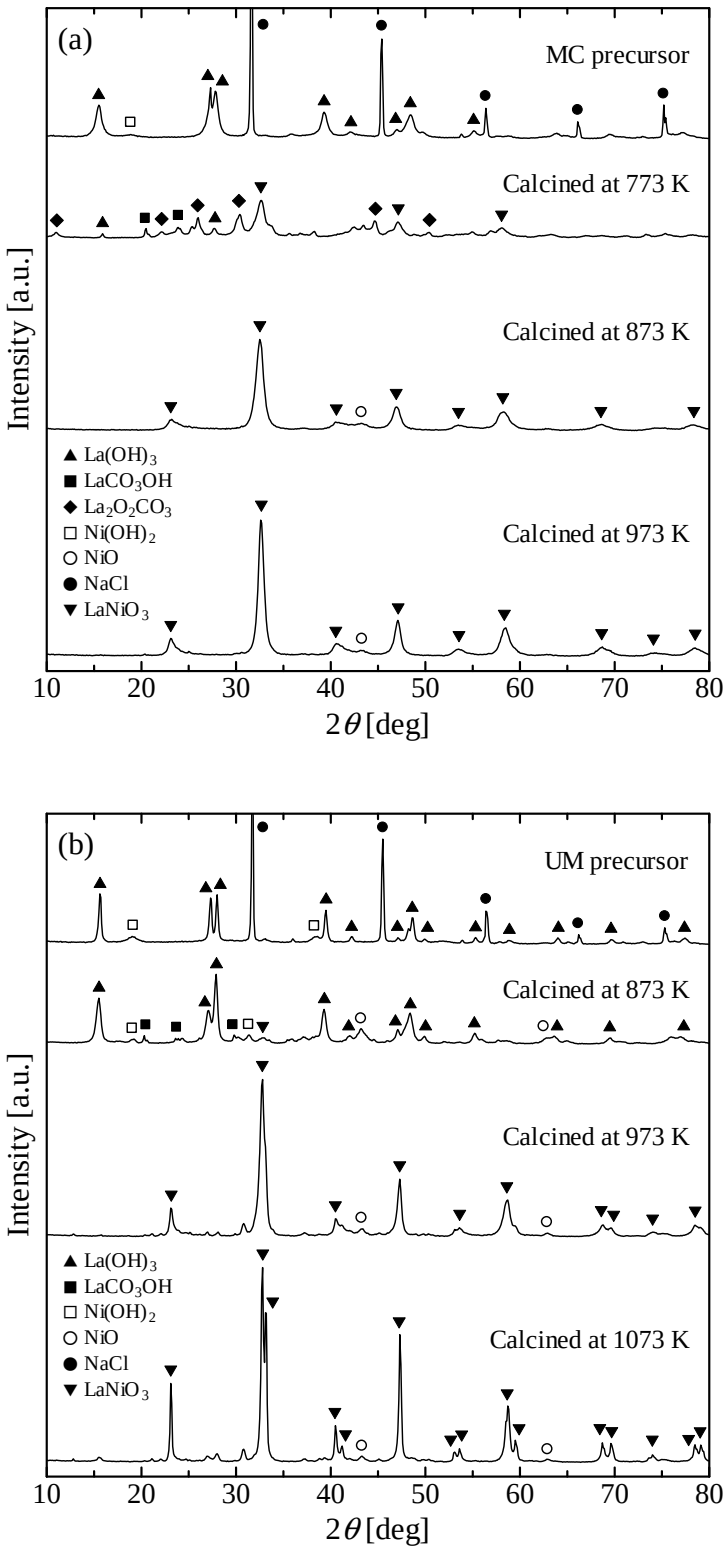

Fig. 3. XRD patterns of final products after calcination of (a) MC and (b) UM precursors at different temperatures.

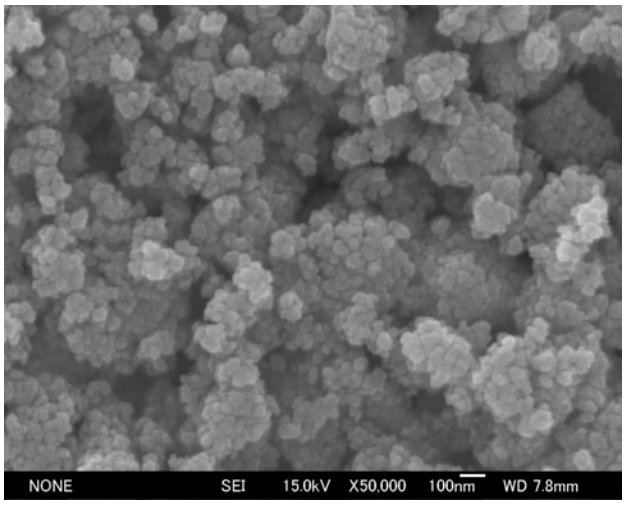

Fig. 4. Typical SEM image of final product derived from MC precursor after calcination at 873 K.

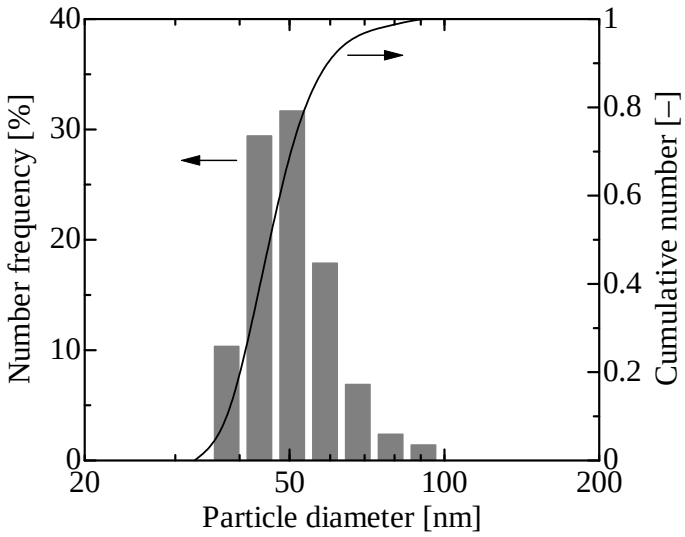

Fig. 5. Particle size distribution of final product derived from MC precursor after calcination at 873 K.

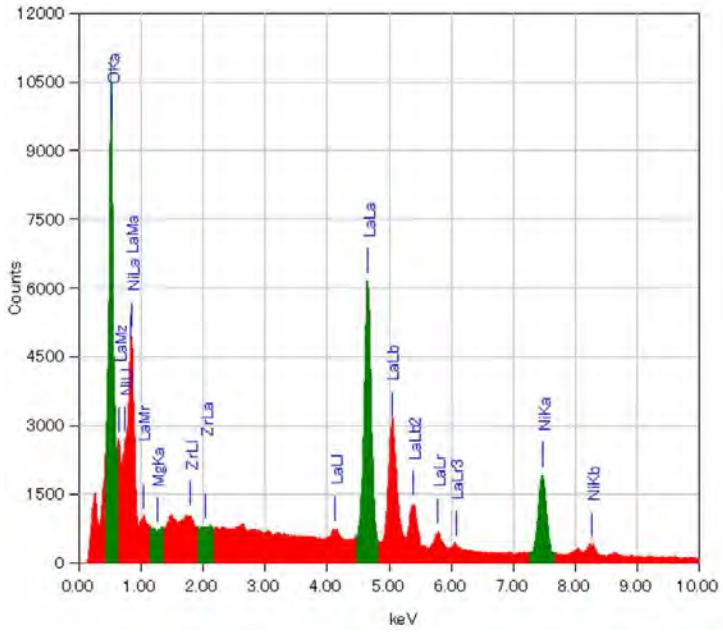

Fig. 6. EDS spectrum of final product derived from MC precursor after calcination at 873 K.

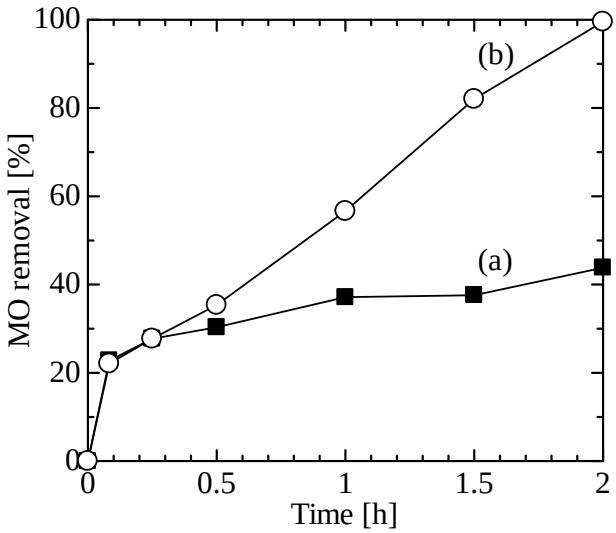

Fig. 7. Removal of MO (a) in the dark and (b) under visible light irradiation using final product derived from MC precursor after calcination at 873 K.